HHS Public Access

Author manuscript

FASEB J. Author manuscript; available in PMC 2023 September 01.

Published in final edited form as:

FASEB J. 2022 September ; 36(9): e22490. doi:10.1096/fj.202101890R.

Near-infrared II photobiomodulation augments nitric oxide bioavailability via phosphorylation of endothelial nitric oxide synthase

Shinya Yokomizo[1,2,*], **Malte Roessing**[3,4,*], **Atsuyo Morita**[4,*], **Timo Kopp**[3,4], **Emiyu Ogawa**[5], **Wataru Katagiri**[6], **Susanne Feil**[3], **Paul L. Huang**[4], **Dmitriy N. Atochin**[4,#], **Satoshi Kashiwagi**[1,#]

[1]Gordon Center for Medical Imaging, Department of Radiology, Massachusetts General Hospital, 149 13th Street, Charlestown, MA, 02129, USA

[2]Department of Radiological Science, Tokyo Metropolitan University, 7-2-10 Higashi-Ogu, Arakawa, Tokyo 116-8551, Japan

[3]Interfaculty Institute of Biochemistry (IFIB), University of Tübingen, Auf der Morgenstelle 34, Tübingen 72076, Germany

[4]Cardiovascular Research Center, Department of Medicine, Massachusetts General Hospital, 149 13th Street, Charlestown, MA 02129, USA

[5]School of Allied Health Science, Kitasato University, 1-15-1 Kitasato Minami-ku Sagamihara, Kanagawa, Japan

[6]Graduate School of Science and Technology, Keio University, 3-14-1 Hiyoshi, Kohoku-ku, Yokohama, Kanagawa 223-8522, Japan

Abstract

There is solid evidence of the beneficial effect of photobiomodulation (PBM) with low-power near-infrared (NIR) light in the NIR-I window in increasing bioavailable nitric oxide (NO). However, it is not established whether this effect can be extended to NIR-II light, limiting broader applications of this therapeutic modality. Since we have demonstrated PBM with NIR laser in the NIR-II window, we determined the causal relationship between NIR-II irradiation and its specific biological effects on NO bioavailability. We analyzed the impact of NIR-II irradiation on NO release in cultured human endothelial cells using a NO-sensitive fluorescence probe and single-cell live imaging. Two distinct wavelengths of NIR-II laser (1064 and 1270 nm) and

[#]**Correspondence should be addressed:** Dmitriy N. Atochin, M.D., Ph.D., Cardiovascular Research Center, Department of Medicine, Massachusetts General Hospital, 149 13th Street, Charlestown, MA 02129, USA, atochin@cvrc.mgh.harvard.edu or Satoshi Kashiwagi, M.D., Ph.D., Gordon Center for Medical Imaging, Department of Radiology, Massachusetts General Hospital, 149 13th Street, Charlestown, MA 02129, USA, Tel: 617-726-6265; skashiwagi@mgh.harvard.edu.

[*]These authors contributed equally.

Author contributions

E.O., P.L.H., D.N.A., and S.K. designed the study; S.Y. and A.M. performed the imaging experiments; S.Y. and W.K. performed the construction of the laser system; S.Y., M.R., A.M. and T.K. performed the image analysis; S.Y., M.R., A.M. and T.K. performed immunoblot analysis and migration assay; S.Y., D.N.A., and S.K. wrote the manuscript; M.R., A.M., T.K., E.O., W.K., S.F. and P.L.H. edited the manuscript.

Disclosures

The authors declare no conflict of interest.

NIR-I (808 nm) at an irradiance of 10 mW/cm^2 induced NO release from endothelial cells. These lasers also enhanced Akt phosphorylation at Ser 473, endothelial nitric oxide synthase (eNOS) phosphorylation at Ser 1177, and endothelial cell migration. Moreover, the NO release and phosphorylation of eNOS were abolished by inhibiting mitochondrial respiration, suggesting that Akt activation caused by NIR-II laser exposure involves mitochondrial retrograde signaling. Other inhibitors that inhibit known Akt activation pathways, including a specific inhibitor of PI3K, Src family PKC, did not affect this response. These two wavelengths of NIR-II laser-induced no appreciable NO generation in cultured neuronal cells expressing neuronal NOS (nNOS). In short, NIR-II laser enhances bioavailable NO in endothelial cells. Since a hallmark of endothelial dysfunction is suppressed eNOS with concomitant NO deficiency, NIR-II laser technology could be broadly used to restore endothelial NO and treat or prevent cardiovascular diseases.

Keywords

photobiomodulation; nitric oxide; endothelial nitric oxide synthase; near-infrared II

1. Introduction

Nitric oxide (NO) is a well-established, multi-functional gaseous mediator to maintain vascular homeostasis (1–4). NO is enzymatically produced by nitric oxide synthase (NOS) *in vivo*. Amongst the known isoforms of NOSs, endothelial NOS (eNOS) is predominantly expressed in endothelial cells and plays an essential role in maintaining the endothelial cell in a quiescent, unactivated state via constant production of the low-level of NO (5, 6). A hallmark of endothelial dysfunction is suppressed eNOS with concomitant NO deficiency; impairment of eNOS activity is implicated in the pathogenesis of cardiovascular diseases (7, 8). Thus, restoring endothelial NO via the modulation of eNOS represents a promising approach to preventing or treating cardiovascular events.

The treatment with low-power near-infrared (NIR) light (630–900 nm) in the NIR-I window has been well established to show diverse biological effects, including analgesia, tissue regeneration, and reduction of inflammation (9–13) and is therefore broadly defined as photobiomodulation (PBM) (11). Notably, PBM has been consistently reported to improve endothelial function via augmenting NO bioavailability (14). First, PBM has been shown to increase NO production from eNOS. 632.5 nm light exposure increased NO generation, proliferation, and migration in endothelial cells and promoted angiogenic activities via eNOS phosphorylation at Ser 1177 (S1177) by Akt kinase and increased eNOS gene expression *in vitro* (15). Second, PBM has been reported to photo-dissociate NO from cytochrome c oxidase (COX) in mitochondria (16–19). NO binds to heme a_3 in competition with oxygen and acts as a reversible inhibitor of COX (20, 21), diverting the fate of oxygen into reactive oxygen species (ROS) formation (18, 22–24), reducing oxygen consumption by inhibition of COX during hypoxia (25), and activating ROS- or NO-mediated signaling (26, 27). 670 nm light exposure has been demonstrated to increase ATP synthase activity via NO dissociation and induce cytoprotective effects in cardiac ischemic injury models *in vivo* (28). Third, PBM can increase NO bioavailability from intracellular stores via actions of heme proteins, including eNOS, COX, hemoglobin, or myoglobin. 590 nm light exposure

has been demonstrated to stimulate nitrate reductase activity of COX and NO release under the hypoxic condition from pre-existing nitrite tissue stores (29, 30). 660 nm light exposure has been similarly shown to release NO from nitrosyl hemoglobin (HbNO) and nitrosyl myoglobin (MbNO) and protected diabetic mice from myocardial infarction, independent of NOS (31). 670 nm light exposure has also been shown to reduce nitrite to form iron-nitrosyl hemoglobin and release NO in blood and muscle (32). NO release from nitrite upon 670 nm light exposure was further confirmed to enhance hindlimb collateralization in a hindlimb ischemia model (33) and cardioprotection in an ischemia-reperfusion model (34).

However, it is yet to be defined whether PBM can be extended to NIR light in the NIR-II window (1000–1700 nm). NIR-II light features the absence of carcinogenic or mutagenic properties (35), reduced scattering, and minimal tissue absorption (36–38), thus achieving the largest penetration depth of 6–8 cm (39) as compared to that of NIR I (~3.2 cm) (40). These features indicate clear advantages of using NIR-II light for a therapeutic purpose over NIR-I. Interestingly, a series of studies demonstrated that low-power NIR-II also shows PBM. NIR-II (1061 to 1301 nm) is reported to augment the immune response to intradermal vaccination and confer protection (41–46). The mechanisms of action involve the generation of ROS and subsequent expression of immunostimulatory chemokines and cytokines in skin cells (41–44, 47). In addition, NIR-II light (1064 nm) exposure has been shown to modify the function of COX and improve tissue oxygenation in humans (48). Although many studies have demonstrated the effect of NIR-I on NO, few studies have been performed on the impact of NIR-II.

We report that non-invasive NIR-II laser exposure increases NO production in endothelial cells via eNOS activation *in vitro*. This method could potentially improve endothelial function via augmenting NO bioavailability and effectively treat cardiovascular diseases.

2 Material and Methods

2.1 Optical Setup

Continuous-wave (CW) Indium gallium arsenide (InGaAs) semiconductor laser diodes (λ = 1064, 1270, or 808 nm, LDX Optronics Inc., USA) were used as sources of NIR light throughout the study (Fig. 1). The laser beam was emitted from a multimode optic fiber (Core: 400 μm, NA: 0.22, Thorlabs, USA) and directed to the bottom of cultured cells by a plano-convex lens (LA1805-C-N-BK7, Thorlabs, USA) and a gold mirror (PF10–03-M01, Thorlabs, USA). To obtain a homogenized flat-top intensity distribution of the beam, we placed a holographic diffuser (47–680, Edmund Optics, USA) under the culture well plate. For the laser radiation safety purpose, an iris was placed in the middle of the optical path, and it was closed during intervals. The laser output was adjusted using a thermal powerhead (S310C and S122C, Thorlabs, USA) and a power meter (PM100D, Thorlabs, USA) to obtain desired irradiances.

2.2 Cell culture

Human umbilical vein endothelial cells (HUVECs) were purchased from ATCC (PCS-100-013, USA) and maintained in Endothelial Cell Growth Medium 2 (EGM2,

C22216, PromoCell GmbH, Germany) with 2% Fetal calf serum and supplements (C39216, PromoCell GmbH) and 1% Penicillin-Streptomycin (Gibco, USA) in a 5% CO2 incubator at 37°C. Cells were used through passage 5. Human neuroblastoma cells (SH-SY5Y, CRL-2266, ATCC) were maintained in Dulbecco's Modified Eagle Medium (Corning, USA) with 10% FBS, 4mM of L-Glutamine (Gibco), and 1% Penicillin-Streptomycin.

2.3 Laser irradiation on endothelial cells and imaging of NO generation

To determine NO generation with NIR laser exposure, we used a NO-sensitive fluorophore to measure NO levels (49). HUVECs were cultured in 24 well plates (Corning) at 60–70% confluency and incubated in a serum-free condition for 70 min. Serum-starved cells were then loaded with 4,5-diaminofluorescein diacetate (DAF-2 DA, Cayman Chemicals, USA) at the final concentration of 5 μM for 60 min at 37°C in serum-free HBSS buffer (Lonza, USA). The cells were then irradiated with 1064, 1270, or 808 nm NIR laser at an irradiance of 0.1–100 mW/cm^2 for 1–5 min. The negligible temperature change of less than 0.6°C in the cell culture area during laser irradiation at an irradiance of up to 100 mW/cm^2, which was the maximum dose used in this study, was confirmed using an infrared (IR) camera (FLIR Systems, USA) (Fig. S1). After the laser exposure, cells were incubated with the complete media for 4 h. Nuclei were stained with NucBlue (Invitrogen, USA) as per the manufacturer's instruction. The signals from DAF-2 and NucBlue were captured using a fluorescence microscopy system (DIAPHOT200, Nikon, Japan) and a CCD digital camera (Hamamatsu Photonics, Japan). Phase-contrast images were also acquired.

To lower NO production, we treated cells with the NOS inhibitor N^5-[imino(nitroamino)methyl]-L-ornithine, methyl ester (L-NAME, 400 μM, Cayman Chemicals), 2-(4-carboxyphenyl)-4,5-dihydro-4,4,5,5-tetramethyl-1H-imidazolyl-1-oxy-3-oxide (c-PTIO, 100 μM, Cayman Chemicals) or calmodulin kinase II inhibitor (NK-93, 100 nM, Selleck Chemicals GmbH, USA) 90 min before the laser treatment. In addition, to determine pathways involved in eNOS phosphorylation, cells were treated 90 min before the laser treatment with potassium cyanide (KCN, 200 nM, Sigma-Aldrich, USA), n-Acetyl-L-cysteine (NAC, 400 μM, RPI Research Products, USA), a PI3K inhibitor (Wortmannin, 10 nM, Calbiochem, USA), an AMPK inhibitor (100 nM, Dorsomorphin, S7306, Selleck Chemicals GmbH), a Src inhibitor (4-Amino-5-(4-methylphenyl)-7-(*t*-butyl)pyrazolo[3,4-*d*]-pyrimidine, PP1, 100 nM, Cayman Chemicals), PKC inhibitor (Gö6983, 10 μM, Calbiochem) or vehicle (DMSO). For positive control of NO production, MAHMA NONOate was used (Cayman Chemicals).

2.4 Image Analysis

The fluorescent intensity of each cell was measured using CellProfiler 4.2.1. (Broad Institute of MIT and Harvard, USA). A published pipeline of "Human cells" was downloaded from https://cellprofiler.org/examples and adjusted for the analysis along with the published methodologies (50, 51). Nuclei were detected from DAPI channel images. Cells were detected from GFP channel images and identified using nuclei data as a reference. The dividing line between cells that couching each other was divided using the propagation algorithm. Determination of the outline of each cell was automatically calculated by thresholding methods, including Otsu or Minimum Cross-Entropy. Inadequate cell images

for the analysis, including those of cells in low viability, out of focus, and active division, were identified using a typical diameter of objects with nuclear counterstaining and excluded from the analysis on the CellProfiler. A fold change of the fluorescence signal intensity at the desired time point over the signal of the control (no laser treatment) was calculated. The fluorescent images were also analyzed using ImageJ (National Institutes of Health, USA). All fluorescence images for a particular fluorophore were normalized identically for all conditions during an experiment. Briefly, the image with the strongest signal was optimized for brightness, contrast, and gamma, and then these settings were applied to all other images acquired for a particular fluorophore.

2.5 Immunocytochemistry analysis

To determine the expression of eNOS and Akt kinase and their phosphorylation status, HUVECs were cultured in Nunc™ Lab-Tek™ II Chamber Slide™ System (Thermo Scientific, USA) with pre-coating of 1:20 gelatin solution (Sigma) in the distilled water (Invitrogen) at 60–70% confluency and incubated in serum-free condition for 1 h. Serum-starved cells were irradiated with 1064 or 1270 nm NIR laser at an irradiance of 10 mW/cm^2 for 5 min. After 30 min incubation in serum-free medium, cells were fixed in 4% paraformaldehyde in phosphate-buffered saline (PBS, Gibco) and permeabilizated in 0.2% Triton X-100 in PBS or Image-iT™ FX Signal Enhancer (Invitrogen). Cells were then incubated with 1% normal goat serum (Jackson ImmunoResearch Laboratories, USA) in 0.1% Tween 20 (Sigma) PBS (TBST) overnight at 4°C. Cells were then incubated with primary antibody overnight at 4°C. The following primary antibodies were used to visualize eNOS, Akt, phospho-eNOS, and phospho-Akt at the dilutions indicated: phospho eNOS (S1177), 1:100 (9570, Cell Signaling Technology, USA); total eNOS, 1:100 (32027, Cell Signaling Technology); phospho Akt (S473), 1:100 (4060, Cell Signaling Technology); total Akt, 1:300 (4691, Cell Signaling Technology). After washing with TBST, cells were incubated with 1:400 Alexa Fluor 488 AffiniPure Goat Anti-Rabbit IgG (H+L) (111-545-144, Jackson ImmunoResearch Laboratories) for 30 min at 4°C. After washing with TBST, slides were mounted using ProLong™ Gold Antifade Mountant with DAPI (Invitrogen). The fluorescence signals were captured using a fluorescence microscopy system and a CCD digital camera. The fluorescent intensity of each cell was measured using ImageJ.

2.6 Immunoblot analysis

To determine the impact of NIR-II laser exposure on Akt and eNOS phosphorylation, we irradiated serum-starved HUVECs with 1064 or 1270 nm NIR laser at an irradiance of 10 mW/cm^2 for 5 min. After 30 min incubation in serum-free medium, cells were washed, lysed with RIPA lysis buffer (Thermo-Fisher Scientific) supplemented with cOmplete Protease Inhibitor Cocktail (Roche, Switzerland) and PhosSTOP (Roche), and scraped from the dish. The lysates were centrifuged, and the protein concentration was determined using a Pierce™ BCA Protein Assay Kit (Thermo-Fisher Scientific) using albumin as a standard. 10–20 μg of protein were suspended in a supplemented 4 × Laemmli Sample Buffer (Bio-Rad, USA) diluted in dH_2O (final concentration: 62.5 mM Tris-HCl, 10% glycerol, 0.0045% bromophenol blue, 1% LDS, and 355 mM ß-2-mercaptoethanol), incubated for 10 min at 85°C. 25–40 uL of diluted samples and 10 uL of Precision Plus Protein™

Kaleidoscope™ Prestained Protein Standards (Bio-Rad) were loaded in NOVEX WedgeWell 8–16% Tris-Glycine Gel 1.0 mm × 10 or 15 well (XP08160BOX or XP08165BOX, Invitrogen). Resolved proteins were transferred to a polyvinylidene difluoride (PVDF) membrane (Millipore Immobilon-P Transfer membrane; Millipore Corp., USA). Following the transfer, the membranes were blocked with 5% bovine serum albumin (BSA) in Tris-buffered saline (TBS) with 1% Tween-20 (TBST) overnight at 4°C. Blocked membranes were then probed with the following primary antibodies for phospho-eNOS (S1177), (9570, Cell Signaling Technology, USA); total eNOS, (32027, Cell Signaling Technology); phospho-Akt (S473), (4060, Cell Signaling Technology); total Akt, (4691, Cell Signaling Technology); and GAPDH (2118, Cell Signaling Technology) diluted with 1% BSA/TBST for 2 h at room temperature. Next, membranes were washed with TBST and incubated with the appropriate secondary antibody conjugated to horseradish peroxidase-conjugated anti-rabbit IgG (111-035-144 Jackson ImmunoResearch, West Grove, PA, USA) for 1 h at room temperature. Antibody binding was visualized using the Pierce™ ECL Western Blotting Substrate (Thermo Fisher Scientific) and imaged using the ChemiDoc MP imaging system (Bio-Rad). Densitometry data were quantified using Image J following established methods (52).

2.7 Cell viability assay

HUVECs were seeded onto 96-well plates at a density of 2×10^3 cells per well. Serum-starved cells were irradiated with 1064 or 1270 nm NIR laser at an irradiance of 10 mW/cm^2 for 5 min. After 24 h incubation in growth media, cell viability was determined using the Cell Counting Kit-8 (CCK-8) from Dojindo Molecular Technologies, Inc., Japan. Briefly, we added 10 μl CCK-8 to each well and incubated the plates for 4 h at 37°C. We measured absorbance at 450 nm using a SpectraMax® M5 (Molecular Devices). We calculated the survival rate as follows: Survival rate (%) = (Asample–Ab)/(Ac−Ab) × 100, where Asample, Ab, and Ac denote the absorbance reading of sample, blanks, and negative control wells, respectively.

2.8 Scratch assay

HUVECs were seeded onto a glass-bottomed dish with an insert (Culture-Insert 2 Well in μ-Dish 35 mm, Ibidi 81176, Germany) at a density of 4×10^5 cells/ml and cultured until they reached confluency. This type of insert allows the creation of a homogeneous cell-free space in the middle of a confluent cell monolayer. We then removed the inserts, serum-starved HUVECs for 30 min, and treated cells with 1064 or 1270 nm NIR laser at an irradiance of 10 mW/cm^2 for 10 min after washing with HBSS buffer to remove cell debris. The cells were incubated for 12 h and imaged using a phase-contrast microscope. Cell migration was evaluated by measuring the cell-free area at the beginning and the surface covered by the cells at the end quantified using ImageJ following the established method (53). Results are expressed as the percentage of wound closure in each experimental group.

2.9 Statistical Analysis

One-way Analysis of Variance (ANOVA) followed by Tukey's multiple comparison tests was performed to compare more than two groups using Prism 9.2.0 (GraphPad software 2021). The mean ± SEM (the standard error of the mean) was displayed for all figures.

A multiple comparison test's corrected P value of less than 0.05 was considered to be significant.

3 Results

3.1 NIR-II promotes NO generation in a dose-dependent manner

NO signaling plays a critical role in endothelial homeostasis (5, 6). We analyzed NO responses in cultured human endothelial cells induced by NIR-II laser exposure using a NO-sensing fluorescence probe. Serum-starved HUVECs, which are known to express abundant eNOS (54), loaded with DAF-2 were irradiated with NIR of 808, 1064, or 1270 nm at an irradiance of 0.1–100 mW/cm^2 for 1–5 min. We compared the fold changes across various laser treatments. In these comparisons, the NIR-II 1064 (Fig. 2A) and 1270 nm (Fig. 2B) laser exposures significantly increased the fluorescence signals. Notably, there was a clear tendency that the relatively low range of 10 mW/cm^2 for 1–5 min 1064 nm laser irradiation had a significant effect (Fig. 2A, the 1064 nm vs. the non-treated control group: $P < 0.0001$ at 1 min and $P = 0.0003$ at 5 min). Similarly, 0.1 mW/cm^2 for 1–5 min (Fig. 2B, the 1270 nm vs. the non-treated control group: $P = 0.0047$ at 1 min and $P < 0.0001$ at 5 min), 1 mW/cm^2 for 1–5 min (Fig. 2B, the 1270 nm vs. the non-treated control group: $P = 0.0377$ at 1 min and $P < 0.0001$ at 5 min), 10 mW/cm^2 for 1–5 min (Fig. 2B, the 1270 nm vs. the non-treated control group: $P < 0.0001$ at 5 min) 1270 nm laser exposure significantly increased NO generation. In contrast, previously reported 0.1–100 mW/cm^2 for 1–5 min exposures with NIR-I 808 nm laser exposure modestly increased NO in endothelial cells (Fig. 2C). No exposure condition induced significant cell death during the experimental time frame (Table S1). These indicate that NIR-II light increases NO production and shows PBM, which is dose-dependent. Therefore, in our following experiments, we chose 10 mW/cm^2 for 5 min of 1064 or 1270 nm laser irradiation. Interestingly, none of these NIR-II lasers increased NO generation in SH-SY5Y human neuroblastoma cell lines (Fig. 2D–E), which are known to express nNOS (55). These results show that the effect of NIR-II is predominantly observed in eNOS positive cells. In addition, these results together suggest that NIR-II shows a superior effect in inducing NO generation to NIR-I. Thus, we focus on the effect of NIR-II on eNOS in endothelial cells in the following investigations.

3.2 NO response to NIR-II exposure involves eNOS phosphorylation

PBM with NIR-I has been established to activate mitochondrial retrograde signaling and increase eNOS phosphorylation at S1177 via activation of Akt kinase (15). Based on this, we determined whether NIR-II induces Akt and eNOS phosphorylation by immunocytochemistry. The 1064 nm laser treatment significantly increased immunoreactivity of S1177 phospho-eNOS compared with that of non-treated cells (Fig. 3A, the 1064 nm vs. the non-treated control group: $P = 0.0002$), while the 1270 nm laser treatment induced a statistically marginal increase. Neither laser treatment showed any impact on eNOS expression level (Fig. 3A). The 1270 nm laser treatment significantly increased immunoreactivity of S473 phospho-Akt compared with that of non-treated cells (Fig. 3B, $P = 0.0012$), while the 1064 nm laser treatment induced a statistically marginal increase (Fig. 3B). Neither laser treatment showed any impact on Akt expression level. These results were also confirmed by immunoblot analysis. Consistently, the 1064 nm

laser treatment resulted in a significant enhancement in phosphorylation of eNOS at S1177 compared with the non-treated control (Fig. 3C, the 1064 nm vs. the non-treated control group: $P = 0.0441$). The 1270 nm laser treatment also increased immunoreactivity of S1177 phospho-eNOS compared with the non-treated control. The 1064 and 1270 nm laser treatment induced an apparent but statistically marginal increase in immunoreactivity of S473 phospho-Akt compared with that of non-treated cells (Fig. 3C). These results suggest that NIR-II exposure induces phosphorylation of Akt and eNOS and increases NO production.

Endothelium-derived NO has been reported to promote endothelial cell proliferation (56, 57). However, exposures of endothelial cells to 1064 nm at 10 mW/cm^2 had no appreciable changes in cell proliferation in this experimental setting (Fig. S2). It has also been well established that endothelium-derived NO and phosphorylation of eNOS at S1177 mediate endothelial cell migration (58, 59). To assess the potential effects of NIR-II exposure on endothelial cell migration, we further performed the scratch wound closure assay. Migration of endothelial cells into the wounded area was significantly increased with the 1064 nm laser treatment at 12 h after wounding compared with the non-laser treated group (Fig. 4, the 1064 nm vs. the non-treated control group: $P = 0.0159$). The 1270 nm laser treatment also induced a statistically marginal increase in migration compared with the non-treated control. These results suggest that increased endothelium-derived NO upon NIR-II exposure can induce functional changes in endothelial cells.

3.3 eNOS phosphorylation is mediated by mitochondrial retrograde signaling

Several signaling pathways have been shown to lie upstream of eNOS phosphorylation. Therefore, we sought to determine the pathway involved in eNOS phosphorylation. HUVECs were treated with PI3K inhibitor (Wortmannin), AMPK inhibitor (Dorsomorphin), Src inhibitor (PP1), or PKC inhibitor (Gö6983) prior to laser treatment. When treated with the pan-eNOS inhibitor, L-NAME, or calmodulin kinase II inhibitor NK-93, or NO scavenger c-PTIO, DAF-2 signal with NIR-II exposure with either 1064 (Fig. 5A, the 1064 nm vs. the L-NAME treated group: $P < 0.0001$, the 1064 nm vs. the NK93 treated group: $P = 0.0003$, the 1064 nm vs. the c-PTIO treated group: $P = 0.0119$) or 1270 nm (Fig. 5B, the 1270 nm vs. the L-NAME treated group: $P = 0.0178$, the 1270 nm vs. the NK93 treated group: $P = 0.0050$, the 1270 nm vs. the c-PTIO treated group: $P < 0.0001$) was markedly decreased, confirming the specificity of NO measurement with the fluorescence probe and eNOS-dependency of NO generation in HUVECs. Treating cells with a PI3K inhibitor, AMPK inhibitor, Src inhibitor, or PKC inhibitor did not result in any appreciable change in NO generation with 1064 or 1270 nm laser exposure (Fig. 5A, 5B). In contrast, treatment with an inhibitor for COX in the mitochondrial respiratory chain, KCN, significantly inhibited NO generation with 1064 (Fig. 5A, the 1064 nm vs. the KCN treated group: $P < 0.0001$) or 1270 nm (Fig. 5B, the 1270 nm vs. the KCN treated group: $P < 0.0001$) laser exposure. It has been well established that PBM is mediated by mitochondrial retrograde signaling, including ROS (10–12, 26, 60–63). NIR light has been shown to alter ROS generation (26, 62) and activate ROS-mediated retrograde signaling via FOXOs, NF-κB, AP-1, and Myc (26). Based on this, we pre-treated cells with NAC, which is a scavenger for superoxide, to suppress this byproduct of oxidative phosphorylation in

mitochondria. Interestingly, upon treating cells with NAC, NO generation with 1064 nm laser exposure was significantly inhibited (Fig. 5A, the 1064 nm vs. the NAC treated group: $P < 0.0001$), indicating that mitochondrial retrograde signaling is involved in NO generation in endothelial cells in response to NIR-II exposure. Consistently, the effect of 1270 nm laser exposure on NO generation was inhibited with NAC treatment (Fig. 5B, the 1270 nm vs. the NAC treated group: $P < 0.0165$), suggesting that the pathway involved in NO generation upon 1270 nm laser exposure is identical to that of 1064 nm.

4 Discussion

In the current study, we have, for the first time, demonstrated that NIR-II laser exposure induces the generation of NO in endothelial cells via Akt and eNOS phosphorylation. Collaborating with known mechanisms of action of PBM, the activation of Akt and eNOS depended on mitochondrial retrograde signaling. Since a hallmark of endothelial dysfunction, leading to cardiovascular diseases, is suppressed eNOS with concomitant NO deficiency, non-invasive NIR-II exposure joins a list of promising modalities to treat cardiovascular diseases. Many therapeutic agents, including NO donors, statins, angiotensin-converting enzyme inhibitors or angiotensin receptor blockers, calcium channel blockers, phosphodiesterase-3 inhibitors, aspirin, dipyridamole, and ellagic acid, have been shown to augment NO bioavailability (7, 8). However, success in clinical trials to treat cardiovascular diseases has remained elusive (64). Therefore, a novel approach to improve endothelial NO bioavailability is desired to reduce morbidity and mortality of cardiovascular diseases. PBM opens the path to achieving this goal; light-based therapy has numerous advantages over conventional pharmacological approaches. First, it is free from cold-chain storage, hypodermic needles, biohazardous sharp waste, irreversible formulation with other ingredients, undesirable biodistribution in vital organs, or unknown long-term toxicity (37, 65, 66). Second, NIR-II light represents a promising therapeutic approach compared to well-established PBM with NIR-I light. The absorption coefficient or the light scattering coefficient in the skin and other tissues decreases slowly with the increase of wavelength and reaches the lowest point around 1125 nm (36). Third, compared to the traditional PBM with NIR I, NIR-II features reduced scattering and minimal tissue absorption (36–38), thus achieving the largest penetration depth (39). These features of NIR-II are more ideal for therapeutic purposes than those of NIR-I.

Our data clearly show that NIR-II laser treatment induces Akt and eNOS phosphorylation. Our group has previously demonstrated three multispectral absorbance peaks in the NIR range: 961, 1319, and 1372 nm in the binding of NO to COX molecule using time-dependent density functional theory (TDDFT) computation (67). These results suggest that the treatment with NIR-II light could result in the photodissociation of NO from COX, exerting PBM in the deep thickness of exposed tissue due to its maximum penetration depth of this range of NIR light in biological tissue (37). Modulation of interactions between COX and NO in mitochondrial electron transport chains has been linked to ROS generation (68). We demonstrated that NIR-II laser modulated intracellular ROS and mitochondrial retrograde signaling in cells (42, 67). Mitochondrial retrograde signaling, including ROS, has been reported to mediate Akt phosphorylation (69, 70). Upon activation of a serine/threonine protein kinase, Akt, also known as protein kinase B, is recruited to the membrane

from the cytosol, where it is phosphorylated in two residues: Thr 308 and Ser 473 (71). Akt then translocates to various sites within the cell and phosphorylates effector substrates, including eNOS (72, 73) to regulate various cellular processes (71). In fact, activation of Akt via ROS has been demonstrated with low-power NIR-I laser treatment (He-Ne laser at 632.8 nm) in cultured cells (74). Although our data (Fig. 5) indicate the involvement of mitochondrial retrograde signaling in NO generation upon NIR-II laser treatment, the detailed pathway(s) to the activation of Akt was not fully elucidated in the current work. Therefore, the exact molecular mechanisms of action of ROS-mediated Akt activation upon NIR-II irradiation await further investigation in the future.

5 Conclusion

Low-power NIR-II lasers of 1064 and 1270 nm enhanced NO generation in human cultured endothelial cells. Akt and eNOS phosphorylation mediates the augmentation of NO generation and endothelial cell migration upon NIR-II exposure via mitochondrial retrograde signaling. A medical laser is well established, and its safety has been well validated in the past decades. Since a hallmark of endothelial dysfunction is suppressed eNOS with concomitant NO deficiency, this laser-based technology could offer a safe and effective choice to restore endothelial NO and treat or prevent cardiovascular diseases.

Supplementary Material

Refer to Web version on PubMed Central for supplementary material.

Acknowledgments

This work was supported by the US NIH grants NIAID #R21AI144103 (S.K.), NINDS #R01NS096237 (D.N.A.) and Massachusetts General Hospital Executive Committee On Research (ECOR) Interim Support Funding (S.K.), the Deutsche Forschungsgemeinschaft (DFG, German Research Foundation) - Projektnummer 335549539 - GRK 2381 (S.F.) and the Reinhard Frank-Stiftung (S.F.). S.Y. was supported by a study abroad scholarship of CMI Inc., Tokyo, Japan. The funders had no role in study design, data collection and analysis, decision to publish, or preparation of the manuscript, and the contents of this paper are solely the responsibility of the authors and do not necessarily reflect the official views of the National Institutes of Health.

Data Accessibility Statement and Data Citation

The datasets generated during the current study are available from the corresponding author on reasonable request.

Non-standard abbreviations:

Akt	Akt serine/threonine protein kinase, Protein kinase B
AMPK	AMP-activated protein kinase
COX	cytochrome c oxidase
c-PTIO	2-(4-carboxyphenyl)-4,5-dihydro-4,4,5,5-tetramethyl-1H-imidazolyl-1-oxy-3-oxide
CW	continuous-wave

DAF-2 DA	4,5-diaminofluorescein diacetate
eNOS	endothelial nitric oxide synthase
HbNO	nitrosyl hemoglobin
HUVECs	Human umbilical vein endothelial cells
InGaAs	Indium gallium arsenide
L-NAME	N^5-[imino(nitroamino)methyl]-L-ornithine, methyl ester
MbNO	nitrosyl myoglobin
NA	Numerical Aperture
NAC	n-Acetyl-L-cysteine
NIR	near-infrared
NO	nitric oxide
nNOS	neuronal nitric oxide synthase
PBM	photobiomodulation
PC	plano-convex
PI3K	phosphoinositide 3-kinases
PKC	protein kinase C
ROS	reactive oxygen species
Ser	serine
SMA	SubMiniature version A
Src	proto-oncogene
TDDFT	time-dependent density functional theory
Thr	threonine

References

1. Stamler JS, Vaughan DE, and Loscalzo J (1989) Synergistic disaggregation of platelets by tissue-type plasminogen activator, prostaglandin E1, and nitroglycerin. Circ Res 65, 796–804 [PubMed: 2504509]
2. Loscalzo J (2001) Nitric oxide insufficiency, platelet activation, and arterial thrombosis. Circ Res 88, 756–762 [PubMed: 11325866]
3. Kawabata A (1996) Evidence that endogenous nitric oxide modulates plasma fibrinogen levels in the rat. British journal of pharmacology 117, 236–237 [PubMed: 8789373]
4. Tousoulis D, Kampoli AM, Tentolouris C, Papageorgiou N, and Stefanadis C (2012) The role of nitric oxide on endothelial function. Curr Vasc Pharmacol 10, 4–18 [PubMed: 22112350]

5. Sobrevia L, Ooi L, Ryan S, and Steinert JR (2016) Nitric Oxide: A Regulator of Cellular Function in Health and Disease. Oxid Med Cell Longev 2016, 9782346 [PubMed: 26798429]

6. Reichenbach G, Momi S, and Gresele P (2005) Nitric oxide and its antithrombotic action in the cardiovascular system. Curr Drug Targets Cardiovasc Haematol Disord 5, 65–74 [PubMed: 15720224]

7. Garry PS, Ezra M, Rowland MJ, Westbrook J, and Pattinson KT (2015) The role of the nitric oxide pathway in brain injury and its treatment--from bench to bedside. Exp Neurol 263, 235–243 [PubMed: 25447937]

8. Srivastava K, Bath PM, and Bayraktutan U (2012) Current therapeutic strategies to mitigate the eNOS dysfunction in ischaemic stroke. Cell Mol Neurobiol 32, 319–336 [PubMed: 22198555]

9. Huang YY, Chen AC, Carroll JD, and Hamblin MR (2009) Biphasic dose response in low level light therapy. Dose Response 7, 358–383 [PubMed: 20011653]

10. Huang YY, Sharma SK, Carroll J, and Hamblin MR (2011) Biphasic dose response in low level light therapy - an update. Dose Response 9, 602–618 [PubMed: 22461763]

11. Karu T (2013) Is it time to consider photobiomodulation as a drug equivalent? Photomed Laser Surg 31, 189–191 [PubMed: 23600376]

12. Karu T (2010) Mitochondrial mechanisms of photobiomodulation in context of new data about multiple roles of ATP. Photomed Laser Surg 28, 159–160 [PubMed: 20374017]

13. Karu TI (2010) Multiple roles of cytochrome c oxidase in mammalian cells under action of red and IR-A radiation. IUBMB life 62, 607–610 [PubMed: 20681024]

14. Quirk BJ, and Whelan HT (2020) What Lies at the Heart of Photobiomodulation: Light, Cytochrome C Oxidase, and Nitric Oxide-Review of the Evidence. Photobiomodul Photomed Laser Surg

15. Chen CH, Hung HS, and Hsu SH (2008) Low-energy laser irradiation increases endothelial cell proliferation, migration, and eNOS gene expression possibly via PI3K signal pathway. Lasers Surg Med 40, 46–54 [PubMed: 18220263]

16. Sarti P, Giuffre A, Forte E, Mastronicola D, Barone MC, and Brunori M (2000) Nitric oxide and cytochrome c oxidase: mechanisms of inhibition and NO degradation. Biochem Biophys Res Commun 274, 183–187 [PubMed: 10903916]

17. Karu TI, and Kolyakov SF (2005) Exact action spectra for cellular responses relevant to phototherapy. Photomed Laser Surg 23, 355–361 [PubMed: 16144476]

18. Boelens R, Wever R, Van Gelder BF, and Rademaker H (1983) An EPR study of the photodissociation reactions of oxidised cytochrome c oxidase-nitric oxide complexes. Biochim Biophys Acta 724, 176–183 [PubMed: 6309220]

19. Boelens R, Rademaker H, Pel R, and Wever R (1982) EPR studies of the photodissociation reactions of cytochrome c oxidase-nitric oxide complexes. Biochim Biophys Acta 679, 84–94 [PubMed: 6275891]

20. Mason MG, Nicholls P, Wilson MT, and Cooper CE (2006) Nitric oxide inhibition of respiration involves both competitive (heme) and noncompetitive (copper) binding to cytochrome c oxidase. Proc Natl Acad Sci U S A 103, 708–713 [PubMed: 16407136]

21. Brown GC, and Cooper CE (1994) Nanomolar concentrations of nitric oxide reversibly inhibit synaptosomal respiration by competing with oxygen at cytochrome oxidase. FEBS letters 356, 295–298 [PubMed: 7805858]

22. Borutaite V, Budriunaite A, and Brown GC (2000) Reversal of nitric oxide-, peroxynitrite- and S-nitrosothiol-induced inhibition of mitochondrial respiration or complex I activity by light and thiols. Biochim Biophys Acta 1459, 405–412 [PubMed: 11004457]

23. Zuckerbraun BS, Chin BY, Bilban M, d'Avila JC, Rao J, Billiar TR, and Otterbein LE (2007) Carbon monoxide signals via inhibition of cytochrome c oxidase and generation of mitochondrial reactive oxygen species. FASEB J 21, 1099–1106 [PubMed: 17264172]

24. Moncada S, and Bolanos JP (2006) Nitric oxide, cell bioenergetics and neurodegeneration. J Neurochem 97, 1676–1689 [PubMed: 16805776]

25. Umbrello M, Dyson A, Feelisch M, and Singer M (2013) The key role of nitric oxide in hypoxia: hypoxic vasodilation and energy supply-demand matching. Antioxid Redox Signal 19, 1690–1710 [PubMed: 23311950]

26. da Cunha FM, Torelli NQ, and Kowaltowski AJ (2015) Mitochondrial Retrograde Signaling: Triggers, Pathways, and Outcomes. Oxid Med Cell Longev 2015, 482582 [PubMed: 26583058]
27. Karu TI, Pyatibrat LV, and Afanasyeva NI (2005) Cellular effects of low power laser therapy can be mediated by nitric oxide. Lasers Surg Med 36, 307–314 [PubMed: 15739174]
28. Zhang R, Mio Y, Pratt PF, Lohr N, Warltier DC, Whelan HT, Zhu D, Jacobs ER, Medhora M, and Bienengraeber M (2009) Near infrared light protects cardiomyocytes from hypoxia and reoxygenation injury by a nitric oxide dependent mechanism. J Mol Cell Cardiol 46, 4–14 [PubMed: 18930064]
29. Ball KA, Castello PR, and Poyton RO (2011) Low intensity light stimulates nitrite-dependent nitric oxide synthesis but not oxygen consumption by cytochrome c oxidase: Implications for phototherapy. J Photochem Photobiol B 102, 182–191 [PubMed: 21237670]
30. Poyton RO, and Ball KA (2011) Therapeutic photobiomodulation: nitric oxide and a novel function of mitochondrial cytochrome c oxidase. Discov Med 11, 154–159 [PubMed: 21356170]
31. Keszler A, Brandal G, Baumgardt S, Ge ZD, Pratt PF, Riess ML, and Bienengraeber M (2014) Far red/near infrared light-induced protection against cardiac ischemia and reperfusion injury remains intact under diabetic conditions and is independent of nitric oxide synthase. Front Physiol 5, 305 [PubMed: 25202275]
32. Hon YY, Sun H, Dejam A, and Gladwin MT (2010) Characterization of erythrocytic uptake and release and disposition pathways of nitrite, nitrate, methemoglobin, and iron-nitrosyl hemoglobin in the human circulation. Drug Metab Dispos 38, 1707–1713 [PubMed: 20634335]
33. Lohr NL, Ninomiya JT, Warltier DC, and Weihrauch D (2013) Far red/near infrared light treatment promotes femoral artery collateralization in the ischemic hindlimb. J Mol Cell Cardiol 62, 36–42 [PubMed: 23702287]
34. Lohr NL, Keszler A, Pratt P, Bienengraber M, Warltier DC, and Hogg N (2009) Enhancement of nitric oxide release from nitrosyl hemoglobin and nitrosyl myoglobin by red/near infrared radiation: potential role in cardioprotection. J Mol Cell Cardiol 47, 256–263 [PubMed: 19328206]
35. Khan I, Tang E, and Arany P (2015) Molecular pathway of near-infrared laser phototoxicity involves ATF-4 orchestrated ER stress. Scientific reports 5, 10581 [PubMed: 26030745]
36. Cao J, Zhu B, Zheng K, He S, Meng L, Song J, and Yang H (2019) Recent Progress in NIR-II Contrast Agent for Biological Imaging. Front Bioeng Biotechnol 7, 487 [PubMed: 32083067]
37. Kashiwagi S, Brauns T, Gelfand J, and Poznansky MC (2014) Laser vaccine adjuvants. History, progress, and potential. Hum Vaccin Immunother 10, 1892–1907 [PubMed: 25424797]
38. Chinnathambi S, and Shirahata N (2019) Recent advances on fluorescent biomarkers of near-infrared quantum dots for in vitro and in vivo imaging. Sci Technol Adv Mater 20, 337–355 [PubMed: 31068983]
39. Dang X, Bardhan NM, Qi J, Gu L, Eze NA, Lin CW, Kataria S, Hammond PT, and Belcher AM (2019) Deep-tissue optical imaging of near cellular-sized features. Scientific reports 9, 3873 [PubMed: 30846704]
40. Chen G, Shen J, Ohulchanskyy TY, Patel NJ, Kutikov A, Li Z, Song J, Pandey RK, Agren H, Prasad PN, and Han G (2012) (alpha-NaYbF4:Tm(3+))/CaF2 core/shell nanoparticles with efficient near-infrared to near-infrared upconversion for high-contrast deep tissue bioimaging. ACS Nano 6, 8280–8287 [PubMed: 22928629]
41. Kimizuka Y, Callahan JJ, Huang Z, Morse K, Katagiri W, Shigeta A, Bronson R, Takeuchi S, Shimaoka Y, Chan MP, Zeng Y, Li B, Chen H, Tan RY, Dwyer C, Mulley T, Leblanc P, Goudie C, Gelfand J, Tsukada K, Brauns T, Poznansky MC, Bean D, and Kashiwagi S (2017) Semiconductor diode laser device adjuvanting intradermal vaccine. Vaccine 35, 2404–2412 [PubMed: 28365253]
42. Kimizuka Y, Katagiri W, Locascio JJ, Shigeta A, Sasaki Y, Shibata M, Morse K, Sirbulescu RF, Miyatake M, Reeves P, Suematsu M, Gelfand J, Brauns T, Poznansky MC, Tsukada K, and Kashiwagi S (2018) Brief Exposure of Skin to Near-Infrared Laser Modulates Mast Cell Function and Augments the Immune Response. J Immunol 201, 3587–3603 [PubMed: 30420435]
43. Morse K, Kimizuka Y, Chan MPK, Shibata M, Shimaoka Y, Takeuchi S, Forbes B, Nirschl C, Li B, Zeng Y, Bronson RT, Katagiri W, Shigeta A, Sirbulescu RF, Chen H, Tan RYY, Tsukada K, Brauns T, Gelfand J, Sluder A, Locascio JJ, Poznansky MC, Anandasabapathy N, and Kashiwagi S (2017)

Near-Infrared 1064 nm Laser Modulates Migratory Dendritic Cells To Augment the Immune Response to Intradermal Influenza Vaccine. J Immunol 199, 1319–1332 [PubMed: 28710250]

44. Kashiwagi S, Yuan J, Forbes B, Hibert ML, Lee EL, Whicher L, Goudie C, Yang Y, Chen T, Edelblute B, Collette B, Edington L, Trussler J, Nezivar J, Leblanc P, Bronson R, Tsukada K, Suematsu M, Dover J, Brauns T, Gelfand J, and Poznansky MC (2013) Near-infrared laser adjuvant for influenza vaccine. PLoS One 8, e82899 [PubMed: 24349390]
45. Khokhlova A, Zolotovskii I, Sokolovski S, Saenko Y, Rafailov E, Stoliarov D, Pogodina E, Svetukhin V, Sibirny V, and Fotiadi A (2019) The light-oxygen effect in biological cells enhanced by highly localized surface plasmon-polaritons. Scientific reports 9, 18435 [PubMed: 31804563]
46. Dolgova D, Abakumova T, Gening T, Poludnyakova L, Zolotovskii I, Stoliarov D, Fotiadi A, Khokhlova A, Rafailov E, and Sokolovski S (2019) Anti-inflammatory and cell proliferative effect of the 1270 nm laser irradiation on the BALB/c nude mouse model involves activation of the cell antioxidant system. Biomed Opt Express 10, 4261–4275 [PubMed: 31453009]
47. Gelfand JA, Nazarian RM, Kashiwagi S, Brauns T, Martin B, Kimizuka Y, Korek S, Botvinick E, Elkins K, Thomas L, Locascio J, Parry B, Kelly KM, and Poznansky MC (2019) A pilot clinical trial of a near-infrared laser vaccine adjuvant: safety, tolerability, and cutaneous immune cell trafficking. FASEB J 33, 3074–3081 [PubMed: 30192655]
48. Wang X, Tian F, Soni SS, Gonzalez-Lima F, and Liu H (2016) Interplay between up-regulation of cytochrome-c-oxidase and hemoglobin oxygenation induced by near-infrared laser. Scientific reports 6, 30540 [PubMed: 27484673]
49. Kojima H, Nakatsubo N, Kikuchi K, Kawahara S, Kirino Y, Nagoshi H, Hirata Y, and Nagano T (1998) Detection and imaging of nitric oxide with novel fluorescent indicators: diaminofluoresceins. Analytical chemistry 70, 2446–2453 [PubMed: 9666719]
50. Stirling DR, Swain-Bowden MJ, Lucas AM, Carpenter AE, Cimini BA, and Goodman A (2021) CellProfiler 4: improvements in speed, utility and usability. BMC Bioinformatics 22, 433 [PubMed: 34507520]
51. Carpenter AE, Jones TR, Lamprecht MR, Clarke C, Kang IH, Friman O, Guertin DA, Chang JH, Lindquist RA, Moffat J, Golland P, and Sabatini DM (2006) CellProfiler: image analysis software for identifying and quantifying cell phenotypes. Genome Biol 7, R100 [PubMed: 17076895]
52. Stael S, Miller LP, Fernandez-Fernandez AD, and Van Breusegem F (2022) Detection of Damage-Activated Metacaspase Activity by Western Blot in Plants. Methods Mol Biol 2447, 127–137 [PubMed: 35583778]
53. Suarez-Arnedo A, Torres Figueroa F, Clavijo C, Arbelaez P, Cruz JC, and Munoz-Camargo C (2020) An image J plugin for the high throughput image analysis of in vitro scratch wound healing assays. PLoS One 15, e0232565 [PubMed: 32722676]
54. Ghigo D, Arese M, Todde R, Vecchi A, Silvagno F, Costamagna C, Dong QG, Alessio M, Heller R, Soldi R, Trucco F, Garbarino G, Pescarmona G, Mantovani A, Bussolino F, and Bosia A (1995) Middle T antigen-transformed endothelial cells exhibit an increased activity of nitric oxide synthase. J Exp Med 181, 9–19 [PubMed: 7528781]
55. Grant MK, Cuadra AE, and El-Fakahany EE (2002) Endogenous expression of nNOS protein in several neuronal cell lines. Life sciences 71, 813–817 [PubMed: 12074940]
56. Ziche M, Morbidelli L, Masini E, Amerini S, Granger HJ, Maggi CA, Geppetti P, and Ledda F (1994) Nitric oxide mediates angiogenesis in vivo and endothelial cell growth and migration in vitro promoted by substance P. J Clin Invest 94, 2036–2044 [PubMed: 7525653]
57. Morbidelli L, Chang CH, Douglas JG, Granger HJ, Ledda F, and Ziche M (1996) Nitric oxide mediates mitogenic effect of VEGF on coronary venular endothelium. Am J Physiol 270, H411–415 [PubMed: 8769777]
58. Murohara T, Witzenbichler B, Spyridopoulos I, Asahara T, Ding B, Sullivan A, Losordo DW, and Isner JM (1999) Role of endothelial nitric oxide synthase in endothelial cell migration. Arterioscler Thromb Vasc Biol 19, 1156–1161 [PubMed: 10323764]
59. Dimmeler S, Dernbach E, and Zeiher AM (2000) Phosphorylation of the endothelial nitric oxide synthase at ser-1177 is required for VEGF-induced endothelial cell migration. FEBS letters 477, 258–262 [PubMed: 10908731]

60. Bohovych I, and Khalimonchuk O (2016) Sending Out an SOS: Mitochondria as a Signaling Hub. Front Cell Dev Biol 4, 109 [PubMed: 27790613]

61. Chandel NS (2015) Evolution of Mitochondria as Signaling Organelles. Cell Metab 22, 204–206 [PubMed: 26073494]

62. Karu TI, Pyatibrat LV, Kolyakov SF, and Afanasyeva NI (2005) Absorption measurements of a cell monolayer relevant to phototherapy: reduction of cytochrome c oxidase under near IR radiation. J Photochem Photobiol B 81, 98–106 [PubMed: 16125966]

63. Karu TI (2008) Mitochondrial signaling in mammalian cells activated by red and near-IR radiation. Photochem Photobiol 84, 1091–1099 [PubMed: 18651871]

64. O'Collins VE, Macleod MR, Donnan GA, Horky LL, van der Worp BH, and Howells DW (2006) 1,026 experimental treatments in acute stroke. Ann Neurol 59, 467–477 [PubMed: 16453316]

65. Kashiwagi S (2020) Laser adjuvant for vaccination. FASEB J 34, 3485–3500 [PubMed: 31994227]

66. Kashiwagi S, Brauns T, and Poznansky MC (2016) Classification of Laser Vaccine Adjuvants. J Vaccines Vaccin 7, 307 [PubMed: 27104047]

67. Katagiri W, Lee G, Tanushi A, Tsukada K, Choi HS, and Kashiwagi S (2020) High-throughput single-cell live imaging of photobiomodulation with multispectral near-infrared lasers in cultured T cells. J Biomed Opt 25, 1–18

68. Sarti P, Forte E, Giuffre A, Mastronicola D, Magnifico MC, and Arese M (2012) The Chemical Interplay between Nitric Oxide and Mitochondrial Cytochrome c Oxidase: Reactions, Effectors and Pathophysiology. Int J Cell Biol 2012, 571067 [PubMed: 22811713]

69. Cairns RA, Harris IS, and Mak TW (2011) Regulation of cancer cell metabolism. Nat Rev Cancer 11, 85–95 [PubMed: 21258394]

70. Panieri E, and Santoro MM (2016) ROS homeostasis and metabolism: a dangerous liason in cancer cells. Cell death & disease 7, e2253 [PubMed: 27277675]

71. Stiles BL (2009) PI-3-K and AKT: Onto the mitochondria. Adv Drug Deliv Rev 61, 1276–1282 [PubMed: 19720099]

72. Namkoong S, Lee SJ, Kim CK, Kim YM, Chung HT, Lee H, Han JA, Ha KS, Kwon YG, and Kim YM (2005) Prostaglandin E2 stimulates angiogenesis by activating the nitric oxide/cGMP pathway in human umbilical vein endothelial cells. Exp Mol Med 37, 588–600 [PubMed: 16391520]

73. Uruno A, Sugawara A, Kanatsuka H, Arima S, Taniyama Y, Kudo M, Takeuchi K, and Ito S (2004) Hepatocyte growth factor stimulates nitric oxide production through endothelial nitric oxide synthase activation by the phosphoinositide 3-kinase/Akt pathway and possibly by mitogen-activated protein kinase kinase in vascular endothelial cells. Hypertension research : official journal of the Japanese Society of Hypertension 27, 887–895 [PubMed: 15824471]

74. Zhang L, Xing D, Gao X, and Wu S (2009) Low-power laser irradiation promotes cell proliferation by activating PI3K/Akt pathway. J Cell Physiol 219, 553–562 [PubMed: 19142866]

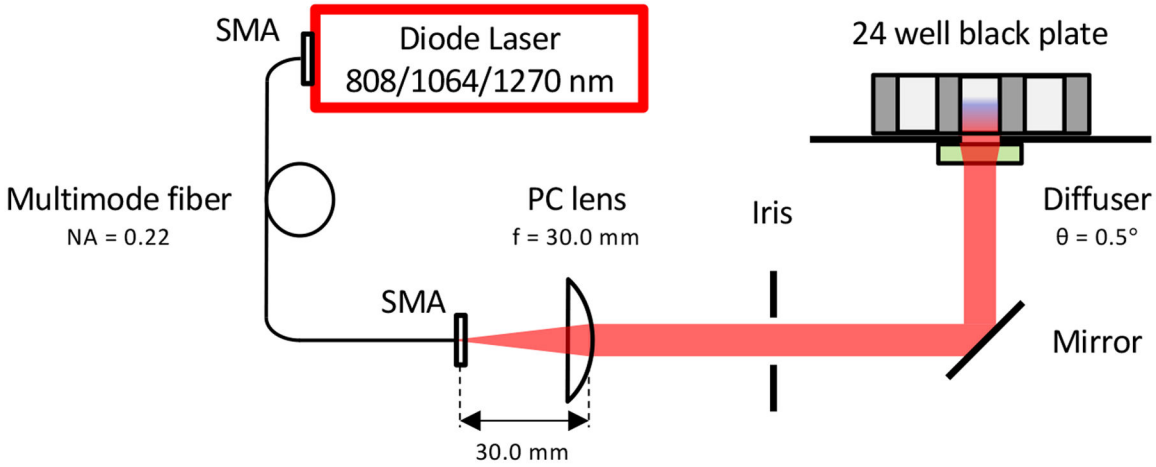

Figure 1. A schematic of the laser irradiation system.

Continuous-wave (CW) InGaAs semiconductor diode laser (λ = 808, 1064, or 1270 nm) was used as a source of near-infrared (NIR) light. The laser beam was emitted from a multimode optic fiber (Core: 400 μm, NA: 0.22) and directed to the bottom of cultured cells by a plano-convex (PC) lens and a gold mirror. A holographic diffuser was placed under the culture well plate. For safety's sake, an iris was placed in the middle of the optical path, and it was closed during intervals. NA: Numerical Aperture, SMA: SubMiniature version A, PC: Plano-Convex.

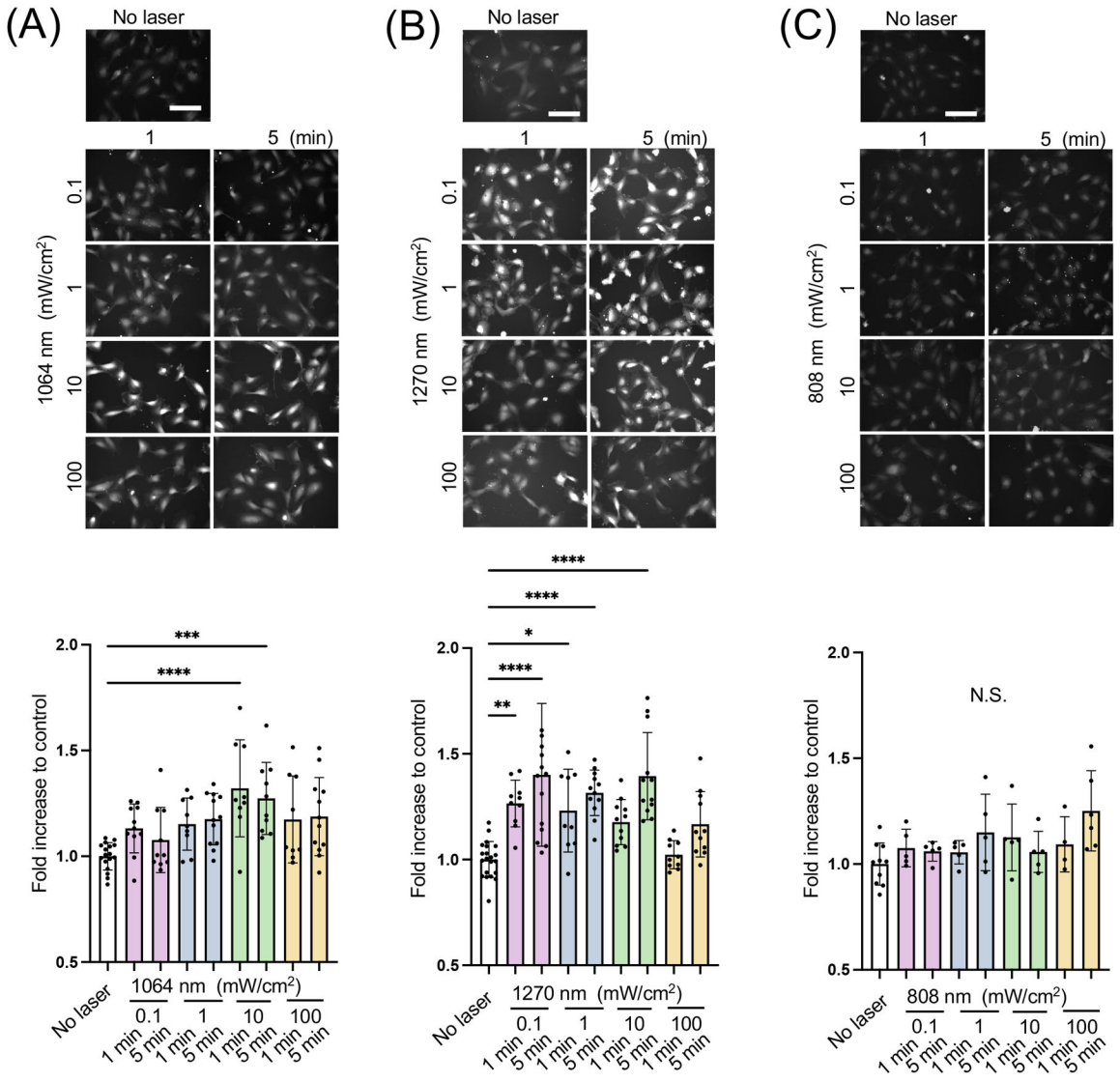

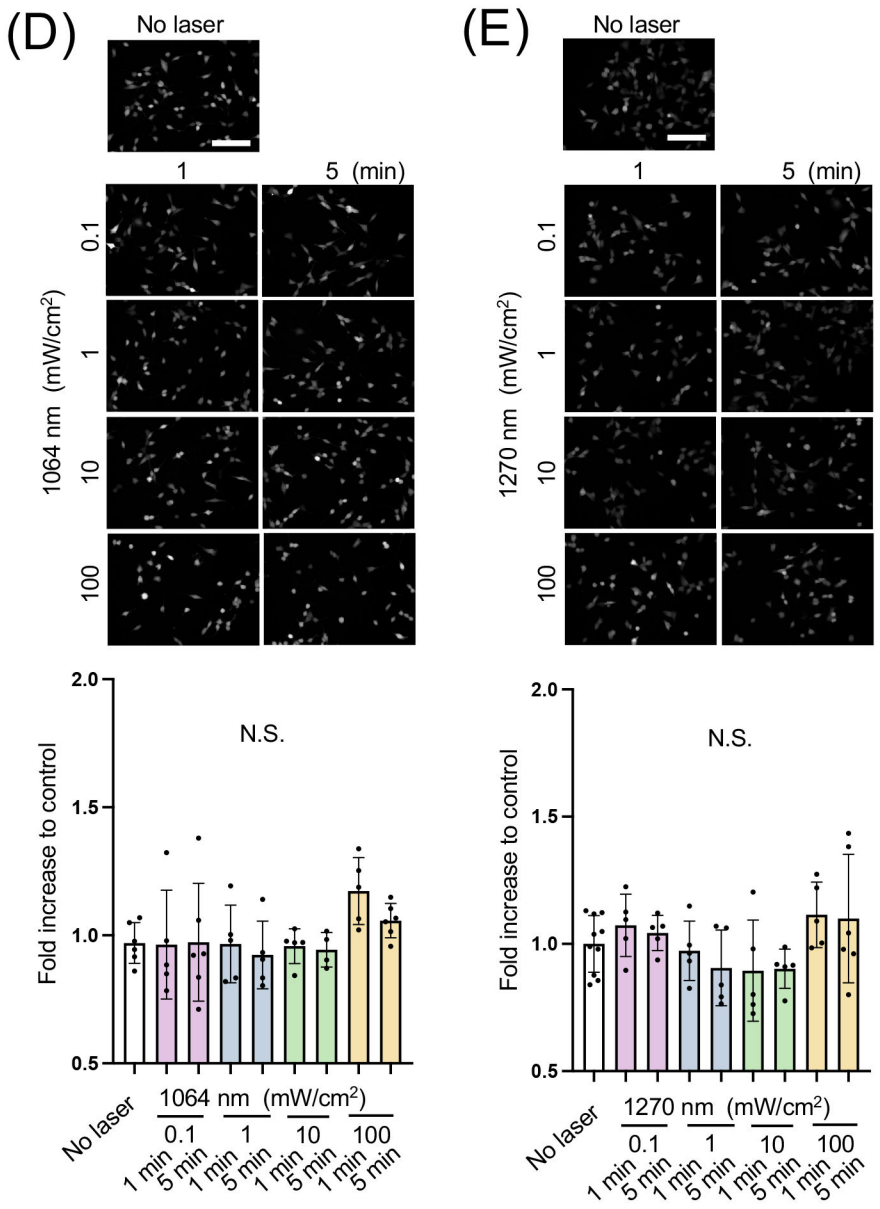

Figure 2. Dose- and time-dependent nitric oxide (NO) generation of human umbilical vein endothelial cells (HUVECs) and neuronal cells induced by NIR-II exposure

A-**C** Cultured HUVECs were exposed to 808, 1064, or 1270 nm laser at an irradiance of 0.1–100 mW/cm^2 for 1–5 min. NO generation was determined using NO-sensitive fluorophore 4,5-diaminofluorescein diacetate (DAF-2 DA). The fold change of the fluorescent signals at each time point over the no laser control group was calculated. **A**-**C** (top) Representative fluorescence images of each experimental group and **A**-**C** (bottom) the fold changes of the signal of **A**, 1064 **B**, 1270 and **C**, 808 nm laser-treatment. **D**-**E** Cultured neuroblastoma cells were also exposed to laser as above. **D**-**E** (top) Representative fluorescence images of each experimental group and **D**-**E** (bottom) the fold changes of the signal of **D**, 1064 and **E**, 1270 nm laser-treatment. Scale bars = 100 μm. **A**-**E**, Results were pooled from three independent experiments. **A**-**C** n = 9–21 **D**-**E** n = 5–10 for each group.

Error bars denote the standard error of the mean (SEM). A P value less than 0.05 was considered significant: * $P < 0.05$; ** $P < 0.01$; *** $P < 0.005$; **** $P < 0.0001$ by one-way ANOVA followed by Tukey's multiple comparison test.

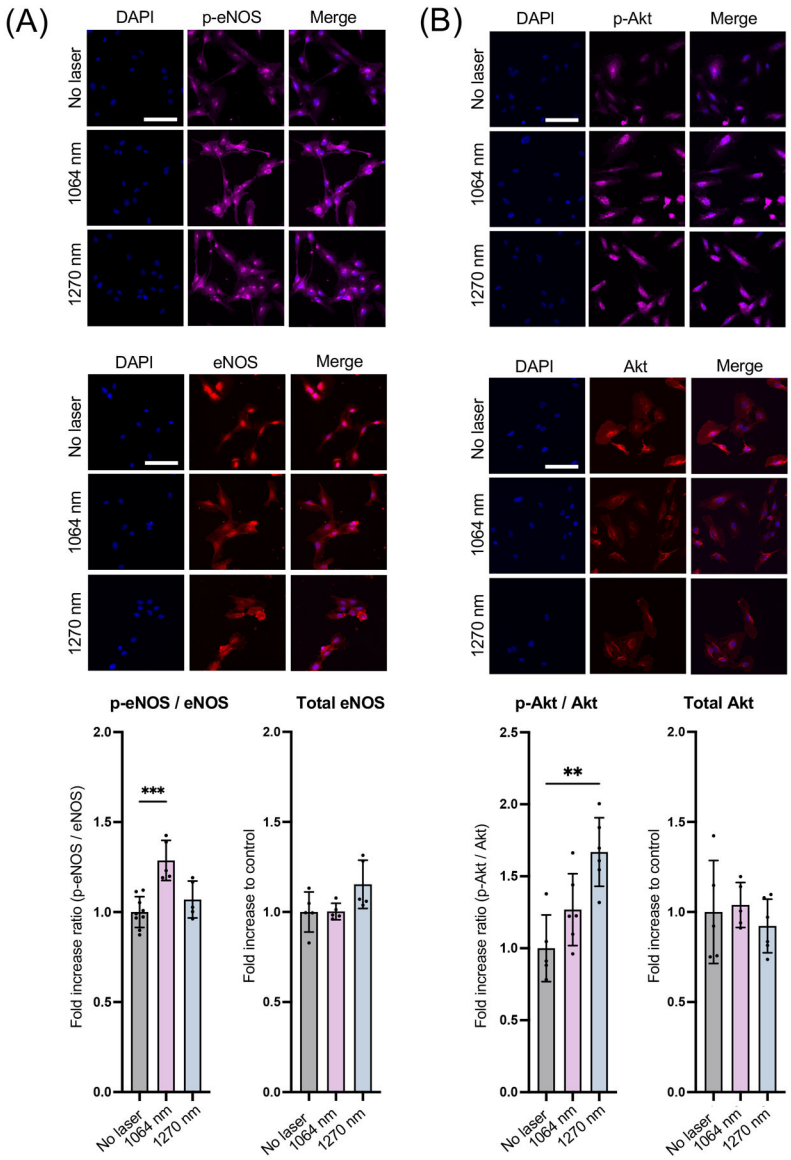

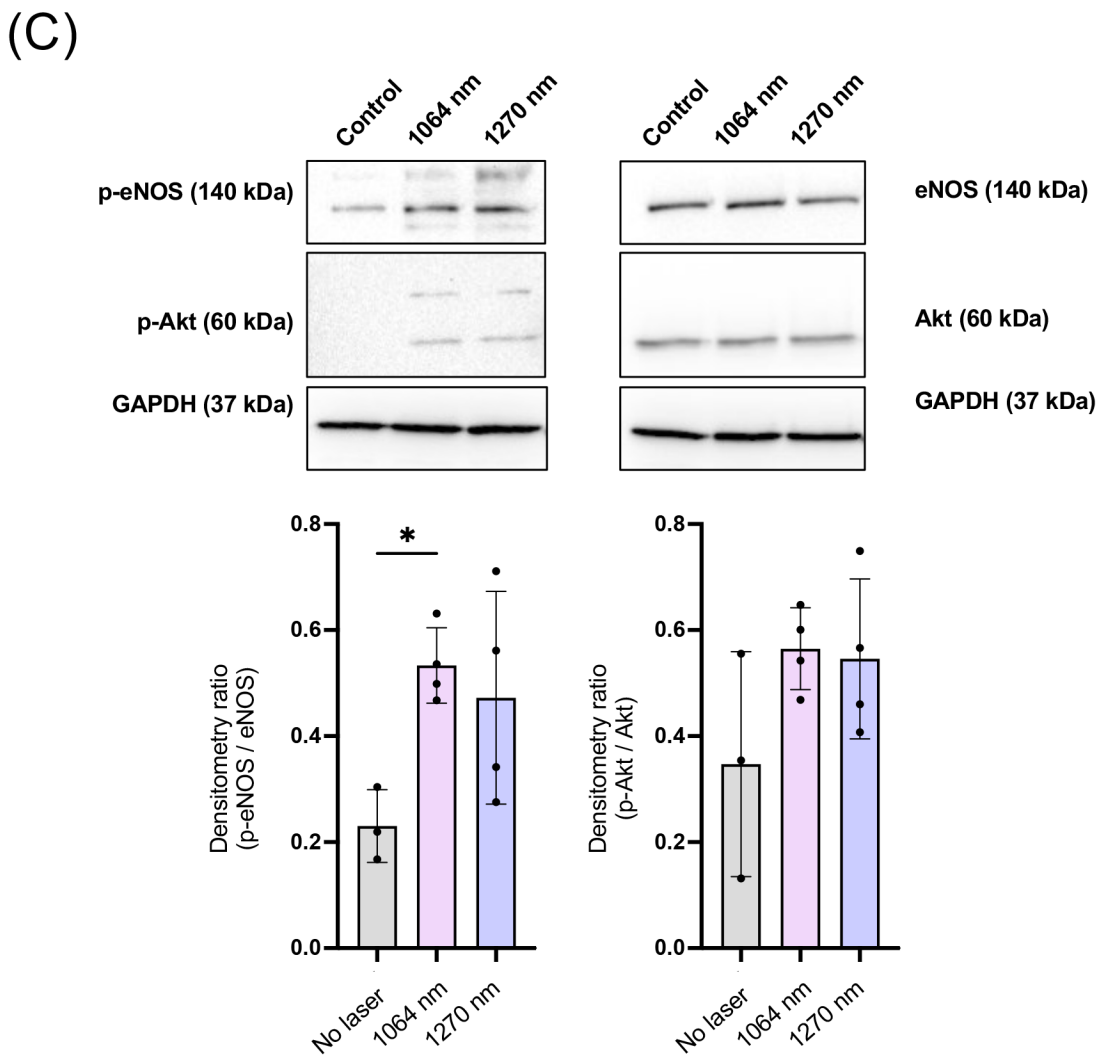

Figure 3. Phosphorylation of endothelial NO synthase (eNOS) and Akt induced by NIR-II exposure

Cultured HUVECs were exposed to 1064 or 1270 nm laser at an irradiance of 10 mW/cm^2 for 5 min. After 30 min incubation in serum-free media, cells were stained with anti-phospho Akt or phospho eNOS, anti-total Akt or eNOS followed by appropriate secondary antibody conjugated to the fluorophore and imaged using an epifluorescence microscope. The fold change of the fluorescent signals at each time point over the no laser control group was calculated. **A**-**B** (top) Representative fluorescence images of the cells immunostained for **A**, total eNOS and phospho-eNOS and **B**, total Akt and phospho-Akt. Scale bars = 100 μm. **A**-**B** (bottom), Quantitative measurements of fold changes in the fluorescence intensity of **A**, p-eNOS and total eNOS and **B**, p-Akt and total Akt. **A**-**B**, Results were pooled from three independent experiments. n = 5–6 cell preparations for each group. **C**, Immunoblot analysis of cultured HUVECs exposed to 1064 or 1270 nm laser at an irradiance of 10 mW/cm^2 for 5 min. After 30 min incubation in serum-free media, cells were lysed, and cell lysates were analyzed by immunoblot analysis. GAPDH was used as the loading control. The membrane was probed with anti-phospho eNOS or anti-phospho Akt,

anti-total eNOS or Akt. **C** (Top), Representative micrographs of the immunoblot analysis. **C** (Bottom), Quantitative measurements of eNOS and Akt phosphorylation by densitometric analysis using ImageJ. Results were pooled from three independent experiments. $n = 3–4$ cell preparations for each group. **A**-**C**, Error bars denote SEM. A P value less than 0.05 was considered significant: * $P < 0.05$; ** $P < 0.01$; *** $P < 0.005$ by one-way ANOVA followed by Tukey's multiple comparison test.

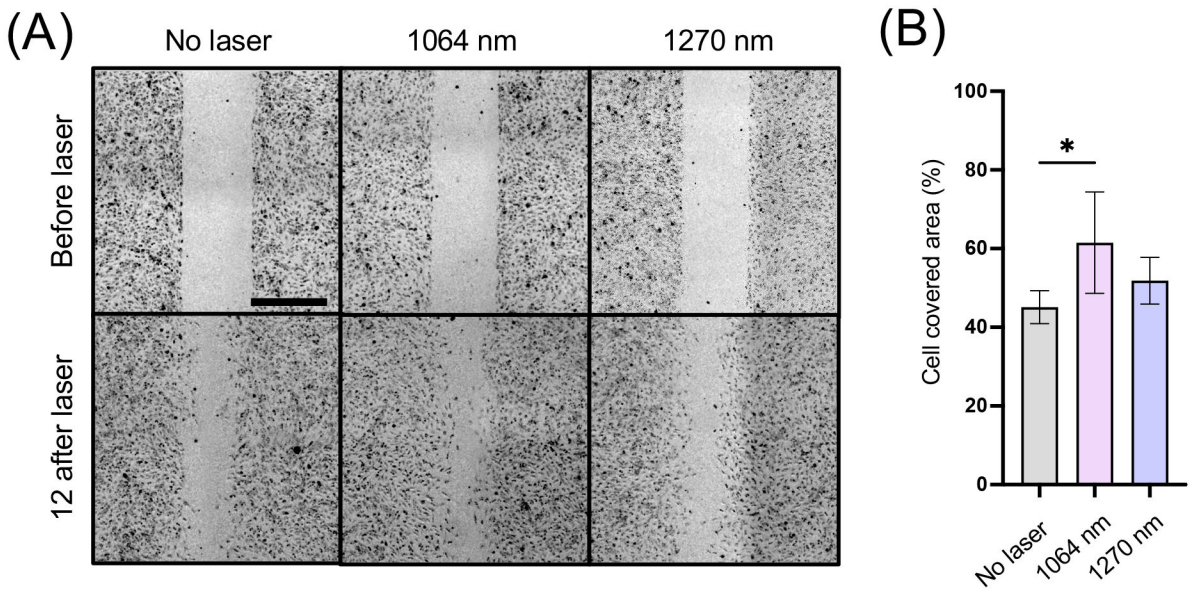

Figure 4. Endothelial migration induced by NIR-II exposure

Cultured HUVECs were serum-starved and treated with 1064 or 1270 nm NIR-II laser at an irradiance of 10 mW/cm^2 for 10 min. **A**, Representative images of scratch assays immediately after the scratches and 12 h after treatment. Scale bars = 500 μm. **B**, Quantitative analysis of the migration area. Results are expressed as the percentage of wound closure in each experimental group. Results were pooled from two independent experiments. n = 5–6 cell preparations for each group. Error bars denote SEM. A P value less than 0.05 was considered significant: * $P < 0.05$ by one-way ANOVA followed by Tukey's multiple comparison test.

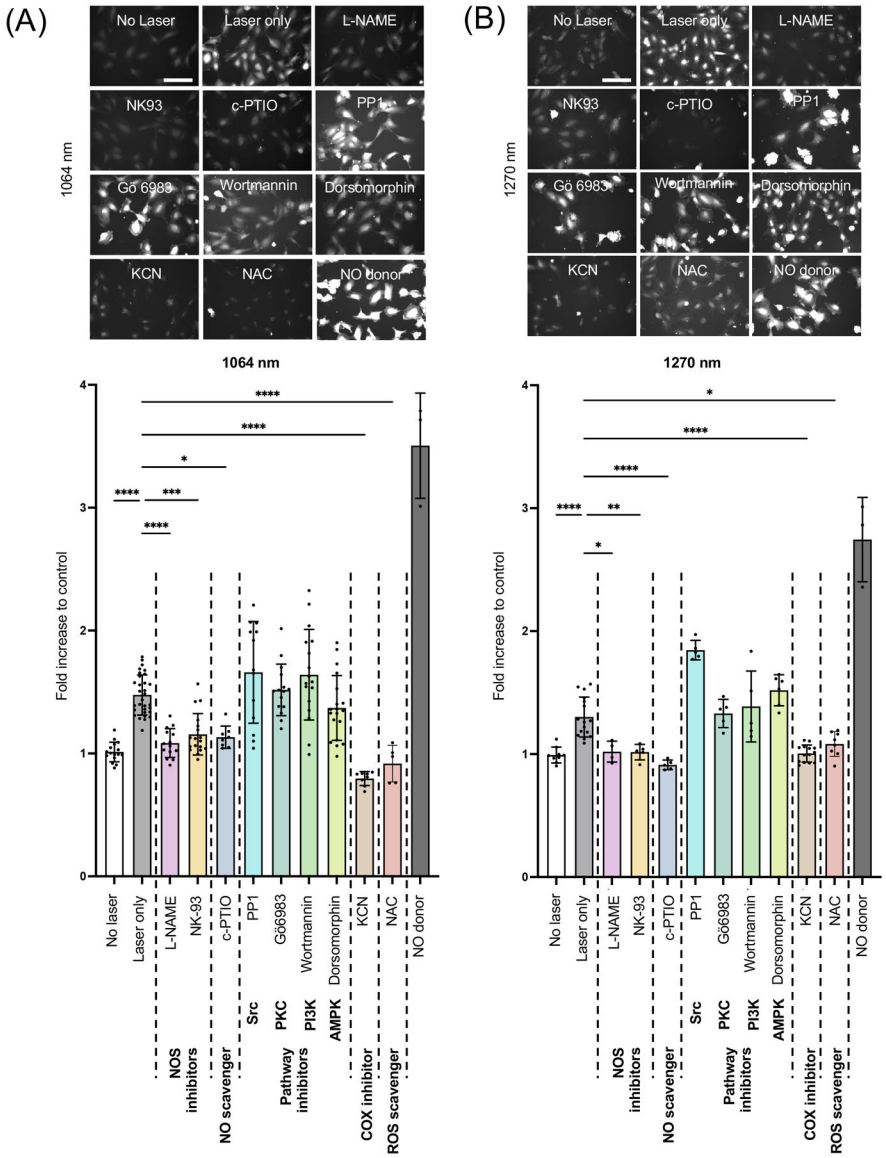

Figure 5. Role of mitochondrial retrograde signaling in NO generation by NIR-II exposure

Cultured HUVECs were serum-starved for 1 h and pre-treated with L-NAME, c-PTIO, NK-93, Wortmannin, Dorsomorphin, PP1, or Gö6983 for 1 h before the laser treatment. Cells were then exposed to 1064 nm laser at an irradiance of 10 mW/cm^2 for 5 min. NO generation was determined using DAF-2 DA. **A**-**B** (top) Representative fluorescence images of each experimental group. Scale bar = 100 μm. **A**-**B** (bottom) Quantitative measurements of fold changes in DAF-2 fluorescence intensity corresponding to the images in A. Results were pooled from three independent experiments. n = 5–31 cell preparations for each group. Error bars denote SEM. A P value less than 0.05 was considered significant: * $P < 0.05$; ** $P < 0.01$; *** $P < 0.005$; **** $P < 0.0001$ by one-way ANOVA followed by Tukey's multiple comparison test.